Malaysian Journal of Chemistry, 2022, Vol. 24(4), 46-58
(Special Issue: *8th International Conference for Young Chemists (ICYC) 2022*)

Physicochemical Properties of Chitosan Modified ZnO QDs and its Feasibility for the Photocatalytic Degradation of Oxytetracycline Under Fluorescent Light Irradiation

Normawati Jasni[1], Anwar Iqbal[1]*, Noor Hana Hanif Abu Bakar[1] and Ahmad Fadly Jusoh[2]
[1]School of Chemical Sciences, Universiti Sains Malaysia, 11800 Gelugor, Penang, Malaysia
[2]Centre For Global Archaeological Research, Universiti Sains Malaysia, 11800 Gelugor, Penang, Malaysia
*Corresponding author (e-mail: anwariqbal@usm.my)

This study reports the synthesis of chitosan-modified ZnO quantum dots (Chitosan-ZnO QDs) via the microwave method for the photodegradation of oxytetracycline (OTC) under visible light irradiation. The synthesised photocatalyst was characterised using Fourier transmission infrared spectroscopy (FT-IR), X-ray diffraction (XRD) analysis, high-resolution transmission electron microscopy (HRTEM), scanning electron microscopy (SEM), UV-vis diffuse reflectance spectroscopy (UV-DRS), photoluminescence (PL) spectroscopy and nitrogen adsorption-desorption (NAD) analysis. The XRD analysis indicates that Chitosan-ZnO QDs have a wurtzite hexagonal crystalline phase with an average crystallite size of 8.2 nm. The SEM analysis shows an evenly distributed micro-spherical structure. The NAD analysis indicates that the Chitosan-ZnO QDs is a mesoporous material with a Brunauer-Emmet-Teller (BET) surface area of 31.88 m^2/g and an average pore size distribution of 11.7 nm. The band gap energy was determined to be 3.29 eV. The PL analysis detected the presence of various defects, enhancing its photocatalytic ability. The removal of OTC was 95.1% within 40 minutes which is higher compared to other ZnO-based photocatalysts reported in the literature. Scavenging tests indicate that photogenerated holes (h^+) and superoxide radicals ($O_2^{\bullet-}$) were the primary reactive oxygen species responsible for photodegrading the OTC. The catalyst was stable to be recycled five times.

Key words: ZnO QDs; chitosan; microwave; photocatalysis; oxytetracycline

Received: October 2022; Accepted: November 2022

Antibiotic contamination in the aquatic environment is a rising concern [1]. Between 100,000 and 200,000 tonnes of antibiotics are consumed yearly to treat various microorganism infections [2]. Oxytetracycline (OTC) is a tetracycline (TC) antibiotic that is employed as a feed additive to promote animal growth in a variety of aquacultures and is widely used to treat human and animal diseases [3]. The widespread use of antibiotics and their frequent discovery endanger human health by fostering the emergence of resistant microorganisms [3]. The advanced oxidation processes (AOP) utilising photocatalysis are identified as the most effective method in removing antibiotics from wastewater compared to other methods such as flocculation, membrane filtration, biological technology, ion exchange and physical adsorption [4-6].

Zinc oxide (ZnO) is stable, biocompatible and cost-effective semiconducting metal oxides [7-8]. However, ZnO responds better to UV light than visible light due to its wide bandgap (3.37 eV) and also having a high rate of charge carrier recombination [9,11]. The high recombination rate reduces the charge carriers' lifespan, significantly reducing its photo-catalytic effectiveness [10].

One efficient way to increase the use of ZnO is to modify the bulk ZnO into zero-dimensional (0D) quantum dots (QDs) [11]. The QDs are nano-crystalline semiconductors with a size of less than 10 nm has a strong confinement effect, hence, making the QDs to possess different physical and chemical properties compared to the bulk counterpart [11-12]. Due to their small size, the electrons are kept in discrete energies quantised states [13]. As a result of quantisation, the band gap is improved as compared to the bulk semiconductor, leading to a large increase in absorption and light emissions [13-14]. These features will allow the QDs to display great photocatalytic features.

The MoS_2/ZnO QDs synthesised by Chen *et al.* [15] was able to remove 96.5% of TC within 80 minutes compared to bare MoS_2 (38.4%) and bulk ZnO (25.6%). In another report, Wahab *et al.* [16] successfully prepared ZnO-QDs to degrade 92% of acetaldehyde within 120 minutes; the efficiencies for Degussa P-25 and ZnO QDs were 70% and 92%, respectively. Also, Mohamed *et al.* [17] reported that the ZnO QDs photocatalytic effectiveness against methyl orange degradation (96%) was twice higher as

†Paper presented at the 8th International Conference for Young Chemists (ICYC) 2022

that of bulk ZnO. The small-sized QDs exhibited greater valence and lowest conduction band and released more energy [15-16].

Surface modification can also create fresh traps on the QDs' surface, increasing the visibility and effectiveness of light-induced reactions on the QDs' surface [18]. Bio-polymer-functioned ZnO has attracted attention in the biomedical and pharmaceutical industries due to its non-toxic and biodegradable characteristics [19]. Among various natural biopolymers, chitosan (poly-1,4, β-D-glucopyranosamine) has gained wide interest due to environmentally friendly, antimicrobial properties, non-mutagenic and economically advantageous manufacturing process because of the hydroxyl and amino functional group of chitosan [19-21]. In photocatalysis, the presence of various functional groups can provide additional adsorption sites and act as trapping sites for pollutants, thereby enhancing photocatalytic activity [22]. In the synthesis of QDs, chitosan can be used to control the growth of particle size and prevent the particles from coagulating. The chitosan backbone's active amine and hydroxyl groups make it possible to bind with metal ions in the formation of ZnO QDs. This provides steric hindrance, which causes stable QDs to develop and improve their suspension in the water [23-24].

Hence, in this study, the microwave method was applied to synthesise chitosan-modified ZnO QDs (Chitosan-ZnO QDs) photocatalyst for the photodegradation of OTC. Upon comparison with other reported photocatalysts, the Chitosan-ZnO QDs displayed better photocatalytic degradation. The dosage required was lower, and the photodegradation reaction took less time in addition to being able to be synthesised through a simple synthesis route.

EXPERIMENTAL

Chemicals and Materials

The following chemicals were purchased from QRëC Chemicals: Zinc acetate dihydrate ($Zn(CH_3COO)_2.2H_2O$, 98%, Grade AR), sulphuric acid (H_2SO_4, 95-97%), isopropanol (IPA, >99%), hydrochloric acid (HCl, 35%), and sodium hydroxide (NaOH, 99%, AR Grade) and Lithium hydroxide (LiOH, 99%, anhydrous). Ascorbic acid (AA, 99%) and potassium bromide salt (KBr, FTIR standard, 99%) and ethylenediaminetetraacetic acid (EDTA, 99.4-100.6%) were purchased from Sigma Aldrich. Whereas absolute ethanol (C_2H_4OH, 99.5%) was from HmBEG Chemical and oxytetracycline dihydrate (OTC, 95%) was from Acros Organic. The chemicals were of analytical grade and were utilised directly. Distilled water was used to prepare all the solutions.

The Preparation of Chitosan-ZnO QDs

The ZnO QDs were synthesised according to Asok *et al.* [25] with some modifications. A LiOH solution was prepared by dissolving 0.0479 g of the LiOH in 20 mL absolute ethanol. Separately, 0.2194 g of zinc acetate was dissolved in 20 mL of absolute ethanol. Both solutions were stirred for 30 minutes before mixing and stirred for another 30 minutes. Then, 25 mg of chitosan flakes were dissolved in 10 mL of (1% v/v) acetic acid under continuous stirring.

The chitosan solution (2 mL) was added to the ZnO QDs solution and stirred for 60 minutes to thoroughly disperse the ZnO QDs into the polymeric solution. The mixture was irradiated with a domestic microwave oven (SAMSUNG/MODEL No: MW61F) for 6 minutes at 100 W. A white precipitate was deposited at the bottom of the beaker when the mixture was cooled to room temperature. The powder was separated from the mother liquor through centrifugation, filtered and washed with ethanol several times to remove unreacted reactants. The sample was dried in an oven at 50 ℃ for 24 hr.

Characterisation of Chitosan-ZnO QDs Catalyst

A Fourier transform infrared (FTIR) spectrometer (Perkin Elmer, System 2000, United States) was used to examine the chemical bonding state of Chitosan-ZnO QDs between the wavelengths of 400-4000 cm^{-1}. The surface morphology was done by scanning electron microscopy (SEM, Quanta FEG-650, United Kingdom). The morphological and particle size distribution was analysed using high-transmission electron microscopy (TECNAI G2 20 S-TWIN, FEI with an accelerating voltage of 200 kV, United States). The structural phases were characterised using an X-ray powder diffractometer (XRD, Bruker D8 Advance, Germany) of Cu Kα irradiation (λ =0.15406 nm) with a scanning rate of 0.02^o min^{-1} and with 2θ from 10-80º. The photoluminescence (Perkin Elmer LS-55, United States) spectra were monitored using fluorescence spectroscopy with a Xenon lamp and 325 nm as the excitation source. The photo-absorption and band gap energy were measured using UV-DRS (a Perkin Elmer Lambda 35 UV/Vis spectrometer, United States). The Brunauer-Emmet-Teller (BET) average surface area of the catalyst was measured by using the instrument Micromeritic ASAP 2020 Surface Adsorption Porosimeter (SAP), United States. The degassing process was conducted at 120 ℃ for 12 hr.

Photocatalytic Activity

The photocatalytic activity was performed in a homemade reactor equipped with two fluorescent

lights (48 W). Using a Dual-Input Data Logging Radiometer (Model PMA 100, Pennsylvania, USA) equipped with visible and UVA+UVB detectors, the light intensity was determined to be 104 W m^{-2}, and the residual UV leakage irradiance of the visible light was measured to be 0.40 W m^{-2}. During the photo-catalytic investigation, 10 mg of the Chitosan-ZnO QDs was dispersed into 50 mL of OTC solution (10 mg L^{-1}) at pH = 9 and stirred vigorously in the dark for 20 minutes to achieve adsorption-desorption equilibrium. The aliquot was collected every 10 minutes, filtered with 0.22 µm membrane filter and measured using the UV-2600, Shimadzu (Japan) spectrometer. The OTC removal efficiency was calculated using the equation (1):

$$\text{OTC degradation (\%R)} = \frac{C_0 - C_t}{C_0} \times 100 \qquad (1)$$

where C_0 and C_t represent the concentration before light irradiation and concentration at a time interval (t, min).

RESULTS AND DISCUSSION

Characterisation

The FTIR spectra of pure chitosan and Chitosan-ZnO QDs are shown in Figure 1. (a). The addition of ZnO QDs changed the vibration and stretching of the chitosan functional groups. The broad and intense absorption band in the range of 3200-3500 cm^{-1} is associated with the surface hydroxyl groups and N-H_2 [26-27]. The band at 2892 cm^{-1} is due to the asymmetric stretching vibration of -CH_2 attributed to the pyranose ring of the chitosan. This peak appears to be less prominent in the spectrum of Chitosan-ZnO QDs [28-29]. This finding is similar to the studies reported by Zabihi *et al.* [30] and Lin *et al.* [27]. The vibrational mode of adsorbed CO_2 from the ambient (air) on the samples' surface may cause the observed band around 2343 cm^{-1} [31]. The band at 2151 cm^{-1} is related to the C-N group of C-NH_2 [32]. The C=O stretching of amide I bonds could be seen at 1644 cm^{-1} [33], whereas the stretching of C-N stretching of amide III can be seen at 1427 cm^{-1} [34]. The intensity of these peaks were observed to be reduced after incorporating ZnO QDs. The stretching vibration of the C-O-C position in the polysaccharide ring of CHT is observed at 1045 cm^{-1} [35, 33]. The reduction in the intensity of this peak after ZnO could indicate the formation of the O-Zn bond [26]. A new absorption band at 511 cm^{-1} in the IR spectrum of Chitosan-ZnO QDs is ascribed to the vibration of group metal-oxygen (Zn-O) bond [19]. The immobilisation of ZnO QDs onto chitosan is shown by a drop in intensities and a band shift [36].

The XRD patterns of Chitosan-ZnO QDs (Figure 1. (b)) match with the wurtzite ZnO (JCPDS card no. 36-1451). The sharpness of the peaks indicates the high purity of the obtained Chitosan-ZnO QDs [37]. A similar finding was reported by Bharathi *et al.* [38] and El-saied *et al.* [39]. The presence of chitosan is indicated by the presence of a broad peak at 2θ = 19.9° [39-42]. However, the XRD peak of chitosan was not observed in this study. The plane of the chitosan could have been destroyed or weakened by the intermolecular hydrogen bonding within the chitosan matrix due to the presence of ZnO, which alters the orientation of the polymer chains [39,42-43].

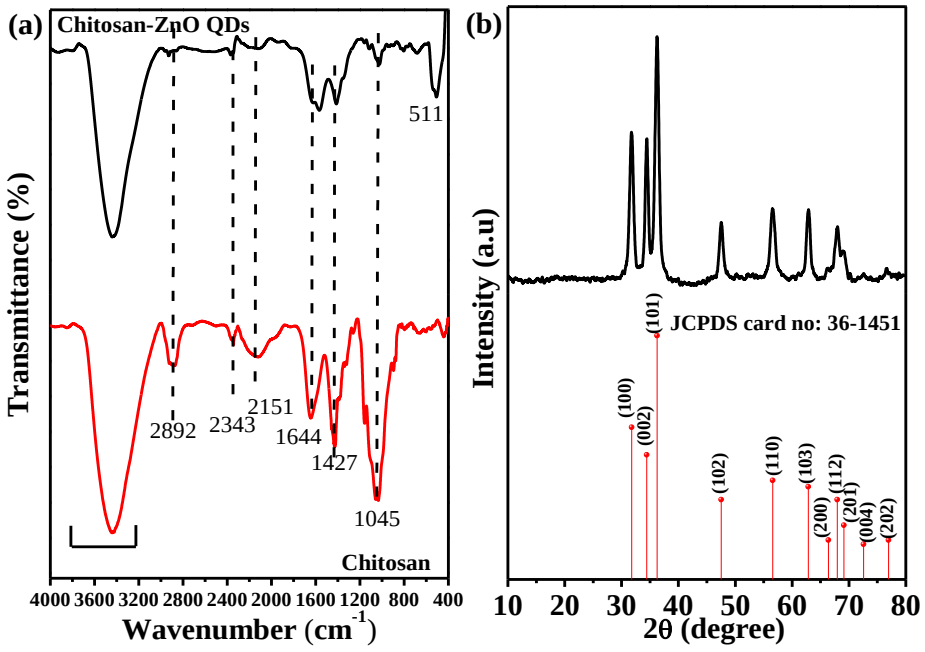

Figure 1. (a) FTIR spectra and (b) XRD pattern

The average crystallite size (D) of Chitosan-ZnO QDs was estimated using the Debye-Scherrer formula, equation (2):

$$D = \frac{K\lambda}{\beta \cos \theta} \quad (2)$$

where K is the Scherrer constant and equals to 0.9, λ presents the wavelength of X-ray radiation, β is the full width at half maximum, and θ is the diffraction angle. The mean crystallite size of 8.2 nm was estimated using the diffraction planes of (100), (002) and (101).

The SEM analysis (Figure 2. (a)) revealed that Chitosan-ZnO QDs have spherically shaped morphology with pores. The architecturally porous material offers a large surface area for adsorption and photodegradation processes, increasing the adsorption of soluble contaminants [44]. The TEM (Figure 2. (b)) analysis showed the presence of spherically shaped particles with an average particle size of 8.84 nm. A histogram indicating the distribution of particle sizes is shown in Figure 2. (c). The d-spacings of (002) and (100) planes at 0.26 nm and 0.28 nm, respectively and were attributed to the wurtzite structure of ZnO (identified from HRTEM analysis (Figure 2. (d)).

The band gap (Eg) of the Chitosan-ZnO QDs and its light absorption evaluated using the UV-DR spectroscopy is presented in Figure 3. (a). The Chitosan-ZnO QDs exhibits a pronounced absorption edge in the ultraviolet (UV) range (389 nm) with low absorption in the visible region [45]. This indicates that Chitosan-ZnO QDs can diffuse the incident light and absorb it repeatedly, which can improve its photocatalytic performance [46].

The Tauc's plot method (insert in Figure 3. (a)) is used to estimate its optical band gap using the following equation (3):

$$(ahv)^2 = A(hv-Eg) \quad (3)$$

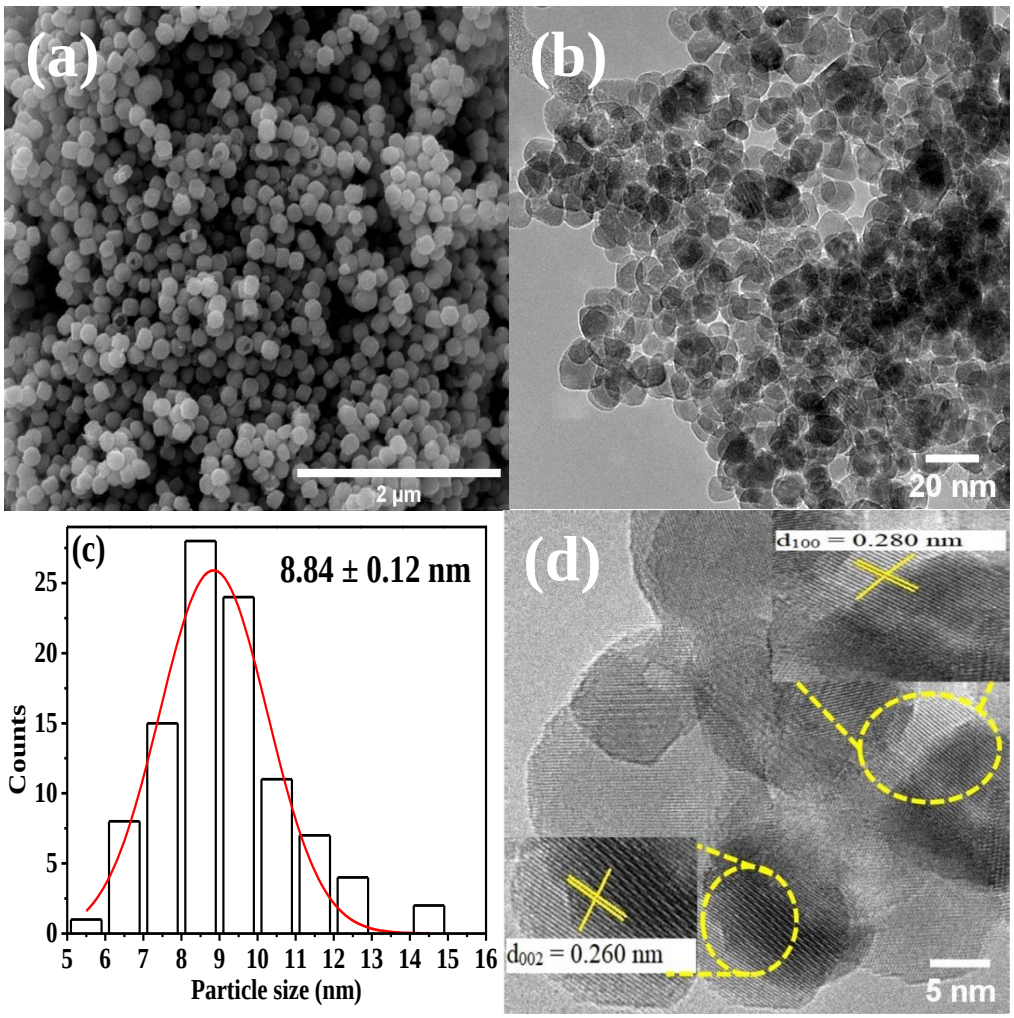

Figure 2. (a) SEM image, (b) TEM image, (c) histogram distribution of particle size, and (d) HRTEM image of Chitosan-ZnO QDs

where A is a constant and a, hv, and Eg are denoted as the absorption coefficient, photon energy, and optical band gap, respectively. The optical band gap is achieved by plotting $(ahv)^2$ versus (hv) and extrapolating the tangent of the curve to $(ahv)^2 = 0$. The band gap energy of Chitosan-ZnO QDs was calculated to be 3.29 eV, which is lower than the reported bulk ZnO band gap (3.37 eV). The narrow band gap energy can lead to more photons being absorbed to create reactive oxidative species and more photogenerated carriers, which would play a big part in photocatalytic activity [47].

The N_2 adsorption-desorption isotherms (Figure 3. (b)) of Chitosan-ZnO QDs correspond to the type IV isotherm as per classification by the International Union of Pure and Applied Chemistry (IUPAC), which is typical for mesoporous materials [22]. The IUPAC classified the hysteresis loop as type H3. The presence of type H3 shows that the pores of Chitosan-ZnO QDs is slit-shaped [40]. The BET specific surface area was estimated at 31.88 $m^2\ g^{-1}$. The Barrett-Joyner-Halenda (BJH) pore size distribution determined from the desorption branch was 11.7 nm and the total pore volume was 0.12 $cm^3\ g^{-1}$.

The PL spectrum with Gaussian curve deconvolution is shown in Figure 3. (c). The UV peak in the PL spectra is theoretically related to band-to-band emission, whereas the visible emission results from defect levels [48]. Defects in quantum dots have recently attracted a lot of interest owing to the energy manifestation levels, which endow them with functionalities including induced carrier trapping, optical absorption, catalysis or electrical properties [49]. The peak at 377 nm is a near-band edge (NBE) transition of ZnO, which corresponds to the recombination of electrons through an exciton collision [50]. The violet and blue emission peaks centred at 406 nm and 451 nm are attributed to the interstitial zinc (Zn_i) and zinc vacancy (V_{Zn}), respectively [51-52]. The green emission peaks centred at 487 and 526 nm are attributed to the oxide antisite (O_{Zn}) and oxygen vacancy (V_o), respectively [53]. Whereas the yellow emission peak centred at 587 nm is oxygen interstitial (O_i) [52].

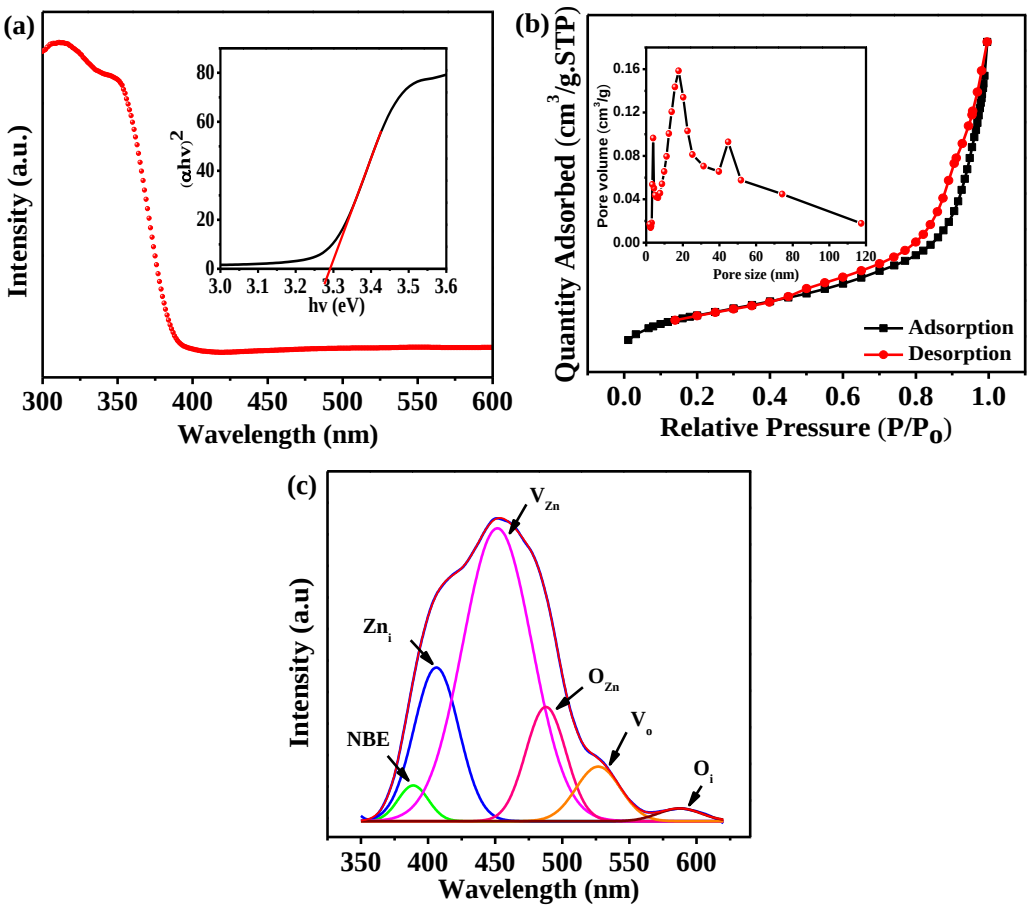

Figure 3. (a) UV-DRS spectra, (b) BET, and (c) deconvoluted of PL spectrum

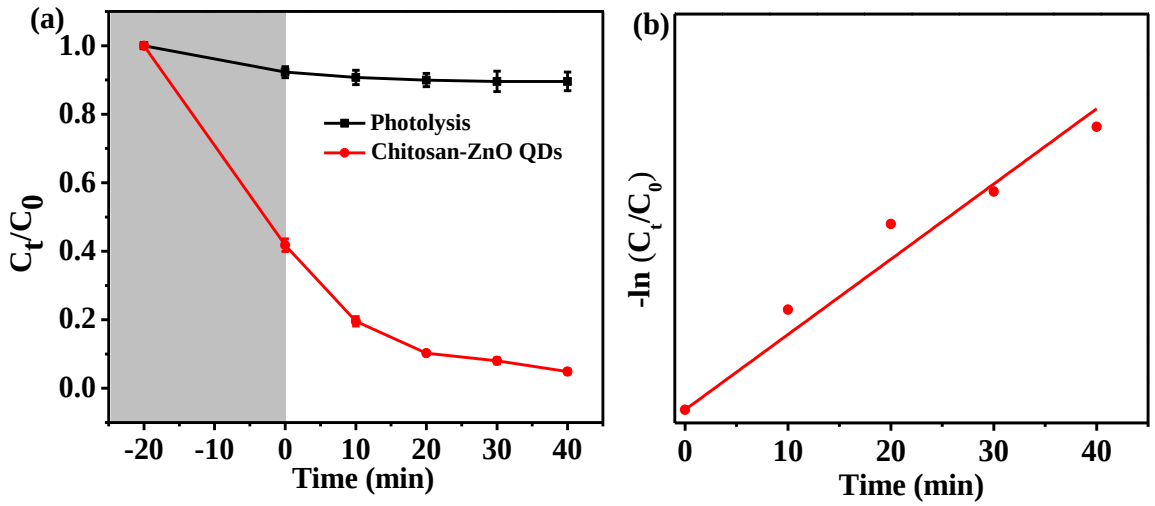

Figure 4. (a) Lowering of C/C_0 vs time due to photodegradation of OTC and (b) determination of rate constant

Photodegradation Study

Photodegradation of OTC

The photocatalytic performance of the Chitosan-ZnO QDs was examined in the photodegradation of OTC under fluorescent light irradiation. The photocatalytic OTC removal profile is shown in Figure 4. (a). From the figure, the concentration of the OTC solution did not noticeably change without any photocatalyst (photolysis), showing its weak capability for self-decomposition [54]. It can be observed that the Chitosan-ZnO QDs have good adsorption capability due to the amine and hydroxyl groups in chitosan can serve as active sites for capturing anionic contaminants. Additionally, the porous structure offers more opportunities for the adsorption/diffusion of substrate molecules and active species during the degradation reaction [55]. The total removal of OTC due to adsorption was 58.2%, whereas the removal percentage increased to 95.1% after irradiation for 40 minutes. The increase shows that a low level of visible light strength is adequate for Chitosan-ZnO QDs to demonstrate its photo-catalytic activity. A greater number of reactive centres, which contribute to amine and hydroxyl groups, leads to more contaminants being adsorbed and speeds up the photocatalytic degradation process. Smaller particle size forms more particles per size unit, hence, increasing the surface area. Higher surface area enriches the interaction with OTC molecules, leading to higher effective degradation [56-57]. Multiple new transfer paths for the photogenerated e^-/h^+ pairs of the photocatalytic material were provided by the surface defects created on the Chitosan-ZnO QDs. This may greatly assist in delaying the process of electron-hole recombination and improving the photocatalytic degradation performance of the material [58,16]. As presented in Figure 4. (b), the photocatalytic degradation kinetics were fitted to a pseudo-first-order kinetic law with reaction rate constants (k) displayed as 0.05705 min^{-1} with a 0.99347 regression coefficient (R^2) value.

The photocatalytic activity of Chitosan-ZnO QDs was compared with the photocatalysts reported in the literature. From Table 1, the photocatalysts show good photocatalytic ability, but a longer reaction time is needed and requires specialised lamps. In addition, the photocatalyst was synthesised through multiple synthesis steps. The Chitosan-ZnO QDs has several advantages compared to the photocatalysts. Chitosan-ZnO QDs can degrade OTC solutions with a comparatively small amount of catalyst, an economical cost experimental setup and a comparatively swift rate of degradation.

Table 1. Comparison of the photocatalytic efficiency of OTC degradation for different photocatalyst

Photocatalyst	Condition	Removal rate	Ref.
p-n heterojunction CdS QDs/$LaMnO_3$ composite	[OTC] = 40 mg L^{-1} Dosage = 400 mg L^{-1} Light source = 300 W high pressure Xe lamp (cut-off wavelength 420 nm)	70.0% after 60 minutes k = 0.01736 min^{-1}	[59]
TiCN	[OTC]= 10 mg L^{-1} Dosage=1000 mg L^{-1} Light source= 200 W LED lamp	97.0% after 300 minutes k = 0.010 min^{-1}	[60]
TiO_2/WO_3	[OTC]= 20 mg L^{-1} Dosage= 500 mg/L Light source= 20 W UVA	100% after 60 minutes k = 0.082 min^{-1}	[61]
CoFe@NSC	[OTC]= 50 mg L^{-1} Dosage= 300 mg L^{-1} Light source= 300 W Xe lamp (λ >400 nm)	82.7 % after 60 minutes k = 0.00886 min^{-1}	[62]
CF/rGO	[OTC]= 10 mg L^{-1} Dosage= 300 mg L^{-1} Light source= 300 W Xe lamp (λ > 420 nm)	84.7% after 40 minutes k = 0.0410 min^{-1}	[63]
BCNNS	[OTC]= 10 mg L^{-1} Dosage=75 mg L^{-1} Light source= 300 W Xe lamp (λ > 420 nm)	72.0% after 60 minutes k= 0.025 min^{-1}	[64]
$Ag/WO_3/g\text{-}C_3N_4$	[OTC]=10 mg L^{-1} Dosage= 400 mg L^{-1} Light source= 500 W Xe lamp	97.74 % after 60 minutes k = 0.1164 min^{-1}	[65]
Dual Z-scheme GCNQDs/ CTO/CFO	[OTC]= 40 mg L^{-1} Dosage= 600 mg L^{-1} Light source= 500 W Xe lamp	88.8% after 150 minutes k = 0.01409 min^{-1}	[66]
Step-scheme $AgInS_2$/ $Agln_5S_8$ heterojunction	[OTC]= 20 mg L^{-1} Dosage=500 mg L^{-1} Light source=300 W Xe lamp (λ >400 nm)	90.5% after 180 minutes k = 0.012 min^{-1}	[67]
$Zn/ZnFe_2O_4$/diatomite	[OTC]= 10 mg L^{-1} Dosage=1000 mg L^{-1} Light source=300 W Xe lamp	95.0% after 150 minutes k = 0.0098 min^{-1}	[68]
ZnO/ZrO_2	[OTC]= 10 mg L^{-1} Dosage=24000 mg L^{-1} Light source=Spectroline XX 15N UV lamp	60.0% after 120 minutes k = 0.0079 min^{-1}	[69]
ZnO NPs	[OTC]= 40 mg L^{-1} Dosage=1000 mg L^{-1} Light source=400 W Halogen lamp	68.0% after 300 minutes k = 0.00299 min^{-1}	[70]
Cu doped ZnO-MWCNT	[OTC]= 50 mg L^{-1} Dosage=500 mg L^{-1} Light source=400 W Halogen lamp	55.0% after 240 minutes k = 0.021 min^{-1}	[71]
Chitosan-ZnO QDs	[OTC]= 10 mg L^{-1} Dosage= 200 mg L^{-1} Light source= 48 W of two compact fluorescent lamp	95.1% after 40 minutes k = 0.05705 min^{-1}	This study

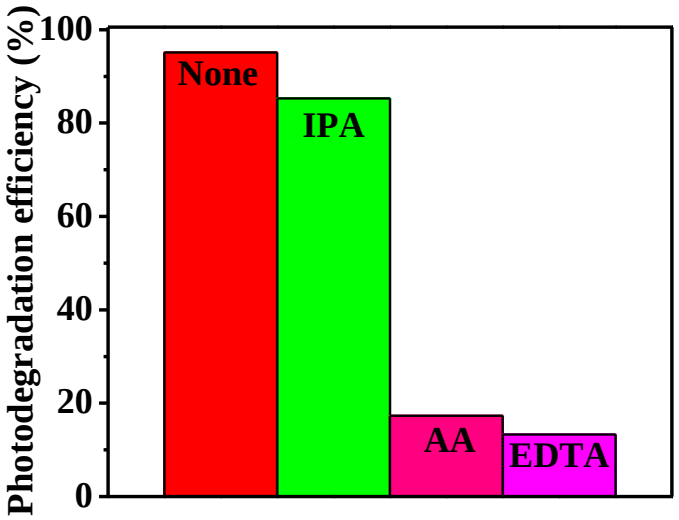

Figure 5. The free radical trapping experiment

Identification of Active Species, Photodegradation Mechanism and Reusability

It is essential to identify the dominant active species to comprehend the photocatalytic mechanism relevant to the degradation of OTC over Chitosan-ZnO QDs. As shown in Figure 5, the removal efficiencies of OTC significantly decreased to 17.3% and 13.3% when AA (the quencher of $O_2^{\bullet-}$) and EDTA (the quencher of h^+) were added, respectively. The IPA (•OH quencher) had little influence on the removal of OTC (85.3%). Hence, it is concluded that $O_2^{\bullet-}$ and h^+ play essential roles in the photodegradation of OTC across the Chitosan-ZnO QDs, whereas •OH play a lesser role.

Chitosan-ZnO QDs' photocatalytic mechanisms were studied by investigating the valence band (VB) and conduction band (CB) positions. The Mulliken electronegativity theory was used to compute the valence band potential (E_{VB}) empirically:

$$E_{VB} = X - E_e + 0.5\ Eg \quad (4)$$

$$E_{CB} = E_{VB} - Eg \quad (5)$$

where Eg and E_e are the band gap of the photocatalyst and electron energy in hydrogen scale (4.5 eV). While X is the electronegativity of ZnO, which is 5.79 eV. The calculated Eg value of Chitosan-ZnO QDs is 3.29 eV. The E_{CB} and E_{VB} were -0.36 eV (in V vs. NHE) and 2.94 eV. Under visible light irradiation, electrons (e^-) will be exited from the VB to the CB, leaving holes (h^+) in the VB. The simultaneous spatial separation and reservation of the useful photogenerated charge carriers with strong redox ability results in high charge-separation efficiency [67]. Since the ECB potential of Chitosan-ZnO QDs (-0.36 eV vs. NHE) is more negative than $E(O_2/O_2^{\bullet-})$ (-0.33 eV vs. NHE), the collected electrons on the CB can reduce surface adsorbed O_2 to produce $O_2^{\bullet-}$ radicals [67]. Since the E_{VB} of Chitosan-ZnO QDs (2.94 eV) is more positive than the standard redox potential of OH^-/H_2O (2.72 eV) and redox potential of H_2O/•OH (2.38 eV vs. NHE) [61], the adsorbed OH^- can be oxidised by reacting with accumulated h^+ in the VB and could react with H_2O to form •OH [59]. Therefore, the efficient degradation of OTC was caused by a significant amount of $O_2^{\bullet-}$ and h^+ and a small amount of •OH radicals. The charge transfer mechanism of the Chitosan-ZnO QDs was presented in Figure 6. (a) in light of the aforementioned experimental findings. The recyclable qualities for OTC photodegradation of the Chitosan-ZnO QDs were also examined. As shown in Figure 6. (b), a slight decrease was observed when the photocatalyst was used repeatedly. The reduction could be caused by the repeated separation process after each cycle and the loss of catalytic material during washing.

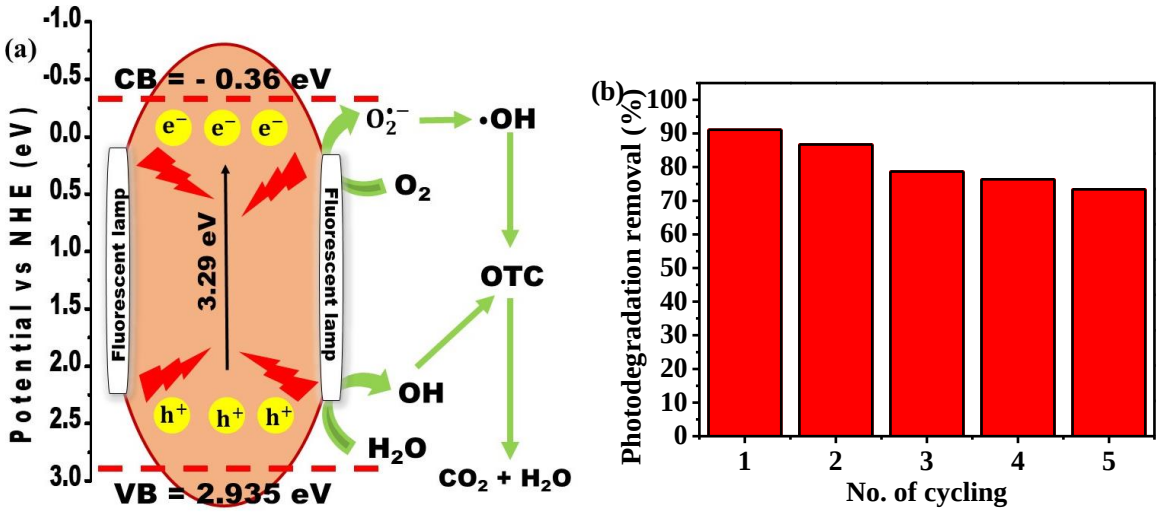

Figure 6. (a) Schematic of the charge transfer and (b) recycling process of photodegradation of OTC

CONCLUSION

Chitosan-modified ZnO quantum dots (Chitosan-ZnO QDs) can be prepared using a microwave method for the photodegradation of OTC under fluorescent light irradiation. The removal of OTC achieved was 95.1% within 40 min, in accordance to the pseudo-first-order kinetic model. The efficient photocatalytic activity of Chitosan-ZnO QDs is attributed to its narrow band gap energy (3.29 eV), which enhanced the light absorption and the presence of various defects. These features slowed down the recombination of photogenerated e^-/h^+ pairs for better generation of photogenerated e^-/h^+ pairs and reactive oxygen species. The photocatalytic degradation of OTC is significantly influenced by h^+ and $O_2^{\bullet-}$. After the fifth cycle, the photocatalyst is still performing admirably.

ACKNOWLEDGEMENTS

We greatly acknowledge the Ministry of Education Malaysia (Higher Education) for the Fundamental Research Grant Scheme (FRGS/1/2019/STG01/USM/02/7).

REFERENCES

1. Chankhanittha, T., Somaudon, V., Photiwat, T., Youngme, S., Hemavibool, K. & Nanan, S. (2021) Enhanced photocatalytic performance of ZnO/Bi_2WO_6 heterojunctions toward photo-degradation of fluoroquinolone-based antibiotics in wastewater. *Journal of Physics and Chemistry of Solids*, **153**, 109995.

2. Li, Z. -J., Qi, W. -N., Feng, Y., Liu, Y. -W, Ebrahim, S. & Long, J. (2019) Degradation mechanisms of oxytetracycline in the environment. *Journal of Integrative Agriculture*, **18(9)**, 1953-1960.

3. Li, C., Zhang, D., Peng, J. & Li, X. (2018) The effect of pH, nitrate, iron (III) and bicarbonate on photodegradation of oxytetracycline in aqueous solution. *Journal of Photochemistry and Photobiology A: Chemistry*, **356**, 239–247.

4. Phoon, B. L., Ong, C. C., Saheed, M. S. M., Show, P. -L., Chang, J. -S., Ling, T. C. & Juan, J. C. (2020) Conventional and emerging technologies for removal of antibiotics from wastewater. *Journal of Hazardous Materials*, **400**, 122961.

5. Gul, I., Sayed, M., Shah, N. S., Khan, J. A., Polychronopoulou, K., Iqbal, J. & Rehman, F. (2020) Solar light responsive bismuth doped titania with Ti^{3+} for efficient photocatalytic degradation of flumequine: Synergistic role of peroxymonosulfate. *Chemical Engineering Journal*, **384**, 123255.

6. Liu, D. -M., Dong, C., Zhong, J., Ren, S., Chen, Y. & Qiu, T. (2020) Facile preparation of chitosan modified magnetic kaolin by one-pot coprecipitation method for efficient removal of methyl orange. *Carbohydrate Polymers*, **245**, 116572.

7. Midya, L., Patra, A. S., Banerjee, C., Panda, A. B. & Pal, S. (2019) Novel nanocomposite derived from ZnO/CdS QDs embedded cross-linked chitosan: An efficient photocatalyst and effective antibacterial agent. *Journal of*

Hazardous Materials, **369**, 398–407.

8. Faisal, M., Harraz, F. A., Jalalah, M., Alsaiari, M., Al-Sayari, S. A. & Al-Assiri, M. S. (2020) Polythiophene doped ZnO nanostructures synthesised by modified sol-gel and oxidative polymerisation for efficient photodegradation of methylene blue and gemifloxacin antibiotic. *Materialstoday Communications,* **24**, 101048.

9. Xu, K., Wu, J., Tan, C. F., Ho, G. W., Wei, A. & Hong, M. (2017) Ag–CuO–ZnO metal–semiconductor multiconcentric nanotubes for achieving superior and perdurable photodegradation. *Nanoscale,* **9(32)**, 11574–11583.

10. Singh, J., Kumar, S., Rishikesh, Manna, A. K. & Soni, R. K. (2020) Fabrication of ZnO–TiO_2 nanohybrids for rapid sunlight driven photodegradation of textile dyes and antibiotic residue molecules. *Optical Materials,* **107**, 110138.

11. Jing, Y., Chen, Z., Ding, E., Yuan, R., Liu, B., Xu, B. & Zhang, P. (2022) High-yield production of g-C_3N_4 quantum dots as photocatalysts for the degradation of organic pollutants and fluorescent probes for detection of Fe^{3+} ions with live cell application. *Applied Surface Science,* **586**, 152812.

12. Guo, Y., Wen, H., Zhong, T., Huang, H. & Lin, Z. (2022) Edge-rich atomic-layered BiOBr quantum dots for photocatalytic molecular oxygen activation. *Chemical Engineering Journal,* **445**, 136776.

13. Kandi, D., Martha, S. & Parida, K. M. (2017) Quantum dots as enhancer in photocatalytic hydrogen evolution: A review. *International Journal of Hydrogen Energy,* **42(15)**, 9467–9481.

14. Mohamed, W., El-Gawad, H. A., Handal, H., Galal, H., Mousa, H., El-Sayed, B. & Labib, A. (2022) Remarkable recycling process of ZnO quantum dots for photodegradation of reactive Yellow dye and solar photocatalytic treatment process of industrial wastewater. *Nanomaterials,* **12(15)**, 2642.

15. Chen, L., Chuang, Y., Chen, C. -W. & Dong, C. -D. (2022) Facile synthesis of MoS_2/ZnO quantum dots for enhanced visible-light photocatalytic performance and antibacterial applications. *Nano-Structures & Nano-Objects,* **30**, 100873.

16. Wahab, R., Tripathy, S. K., Shin, H. -S., Mohapatra, M., Musarrat, J., Al-Khedhairy, A. A. & Kaushik, N. K. (2013) Photocatalytic oxidation of acetaldehyde with ZnO-quantum dots. *Chemical Engineering Journal,* **226**, 154–160.

17. Mohamed, W. A. A., Ibrahem, I. A., El-Sayed, A. M., Galal, H. R., Handal, H., Mousa, H. A. & Labib, A. A. (2020) Zinc oxide quantum dots for textile dyes and real industrial wastewater treatment: Solar photocatalytic activity, photoluminescence properties and recycling process. *Advanced Powder Technology,* **31(6)**, 2555–2565.

18. Rajabi, H. R. (2016) Photocatalytic Activity of Quantum Dots. In (Ed.), Semiconductor Photocatalysis - Materials, Mechanisms and Applications. IntechOpen.

19. Preethi, S., Abarna, K., Nithyasri, M., Kishore, P., Deepika, K., Ranjithkumar, R. & Bharathi, D. (2020) Synthesis and characterisation of chitosan/zinc oxide nanocomposite for antibacterial activity onto cotton fabrics and dye degradation applications. *International Journal of Biological Macromolecules,* **164**, 2779–2787.

20. Asgari-Targhi, G., Iranbakhsh, A., Ardebili, Z. O. & Tooski, A. H. (2021) Synthesis and characterisation of chitosan encapsulated zinc oxide (ZnO) nanocomposite and its biological assessment in pepper (Capsicum annuum) as an elicitor for in vitro tissue culture applications. *International Journal of Biological Macromolecules,* **189**, 170–182.

21. Gasti, T., Dixit, S., Hiremani, V. D., Chougale, R. B., Masti, S. P., Vootl, S. K. & Mudigoudra, B. S. (2022) Chitosan/pullulan based films incorporated with clove essential oil loaded chitosan-ZnO hybrid nanoparticles for active food packaging. *Carbohydrate Polymers,* **277**, 118866.

22. Adnan, M. A. M., Phoon, B. L., Johan, M. R., Tajaruddin, H. A. & Julkapli, N. M. (2022) Visible light-enable oxidation and antibacterial of zinc oxide hybrid chitosan photocatalyst towards aromatic compounds treatment. *Materialstoday Communications,* **32**, 103956.

23. Kameda, T., Honda, R., Kumagai, S., Saito, Y. & Yoshioka, T. (2019) Uptake of heavy metal cations by chitosan-modified montmorillonite:

Kinetics and equilibrium studies. *Materials Chemistry and Physics*, **236**, 121784.

24. Saeed, S. E. -S., El-Molla, M. M., Hassan, M. L., Bakir, E., Abdel-Mottaleb, M. M. S. & Abdel-Mottaleb, M. S. A. (2014) Novel chitosan-ZnO based nanocomposites as luminescent tags for cellulosic materials. *Carbohydrate Polymers*, **99**, 817–824.

25. Asok, A. (2013) Microwave accelerated one-minute synthesis of luminescent ZnO quantum dots. *AIP Conference Proceedings*, **1512(1)**, 404.

26. Zhong, R., Zhong, Q., Huo, M., Yang, B. & Li, H. (2020) Preparation of biocompatible nano-ZnO/chitosan microspheres with multi-functions of antibacterial, UV-shielding and dye photo-degradation. *International Journal of Biological Macromolecules*, **146**, 939–945.

27. Lin, M. -H., Wang, Y. -H., Kuo, C. -H., Ou, S. -F., Huang, P. -Z., Song, T. -Y., & Fan, F. -Y. (2021) Hybrid ZnO/chitosan antimicrobial coatings with enhanced mechanical and bioactive properties for titanium implants. *Carbohydrate Polymers*, **257**, 117639.

28. Rahman, P. M., Mujeeb, V. M. A., Muraleedharan, K. & Thomas, S. K. (2018) Chitosan/nano ZnO composite films: Enhanced mechanical, anti-microbial and dielectric properties. *Arabian Journal of Chemistry*, **11(1)**, 120–127.

29. A, A., Samad, S. A., Huq, D., Moniruzzaman, M. & Masum, S. M. (2013) Textile dye removal from wastewater effluents using Chitosan-ZnO nanocomposite. *Journal of Textile Science & Engineering*, **5**,3.

30. Zabihi, E., Babaei, A., Shahrampour, D., Arab-Bafrani, Z., Mirshahidi, K. S. & Majidi, H. J. (2019) Facile and rapid in-situ synthesis of chitosan-ZnO nano-hybrids applicable in medical purposes; a novel combination of bio-mineralisation, ultrasound, and bio-safe morphology-conducting agent. *International Journal of Biological Macromolecules*, **131**, 107–116.

31. Zabihi, E., Arab-Bafrani, Z., Hoseini, S. M., Mousavi, E., Babaei, A., Khalili, M. & Javid, N. (2021) Fabrication of nano-decorated ZnO-fibrillar chitosan exhibiting a superior performance as a promising replacement for conventional ZnO. *Carbohydrate Polymers*, **274**, 118639.

32. Ali, M. E. A., Aboelfadl, M. M. S., Selim, A. M., Khalil, H. F. & Elkady, G. M. (2018) Chitosan nanoparticles extracted from shrimp shells, application for removal of Fe(II) and Mn(II) from aqueous phases. *Separation Science and Technology*, **53(18)**, 2870–2881.

33. Masud, R. A., Islam, M. S., Haque, P., IKhan, M. N., Shahruzzaman, M., Khan, M., & Rahman, M. M. (2020) Preparation of novel chitosan/poly (ethylene glycol)/ZnO bionanocomposite for wound healing application: Effect of gentamicin loading. *Materialia*, **12**, 100785.

34. Kumar, S., Ye, F., Mazinani, B., Dobretsov, S. & Dutta, J. (2021) Chitosan nanocomposite coatings containing chemically resistant ZnO–SnOx core–shell nanoparticles for photocatalytic antifouling. *International Journal of Molecular Sciences*, 22(9), 4513.

35. Haldorai, Y. & Shim, J. -J. (2013) Chitosan-Zinc Oxide hybrid composite for enhanced dye degradation and antibacterial activity. *Composite Interfaces*, **20(5)**, 365–377.

36. Türemen, M., Demir, A. & Gokce, Y. (2021) The synthesis and application of chitosan coated ZnO nanorods for multifunctional cotton fabrics. *Materials Chemistry and Physics*, **268**, 124736.

37. Yadollahi, M., Farhoudian, S., Barkhordari, S., Gholamali, I., Farhadnejad, H., & Motasadizadeh, H. (2016) Facile synthesis of chitosan/ZnO bio-nanocomposite hydrogel beads as drug delivery systems. *International Journal of Biological Macromolecules*, **82**, 273–278.

38. Bharathi, D., Ranjithkumar, R., Chandarshekar, B. & Bhuvaneshwari, V. (2019) Preparation of chitosan coated zinc oxide nanocomposite for enhanced antibacterial and photocatalytic activity: As a bionanocomposite. *International Journal of Biological Macromolecules*, **129**, 989-996.

39. El-saieda, H. A. -A. & Ibrahim, A. M. (2020) Effective fabrication and characterization of eco-friendly nano chitosan capped zinc oxide nanoparticles for effective marine fouling inhibition. *Journal of Environmental Chemical Engineering*, **8(4)**, 103949.

40. Priyadarshi, G., Raval, N. P. & Trivedi, M. H. (2022) Microwave-assisted synthesis of cross-linked chitosan-metal oxide nanocomposite for methyl orange dye removal from unary and

complex effluent matrices. *International Journal of Biological Macromolecules,* **219**, 53–67.

41. Chelu, M., Moreno, J. C., Atkinson, I., Cusu, J. P., Rusu, A., Bratan, V. & Musuc, A. M. (2022) Green synthesis of bioinspired chitosan-ZnO-based polysaccharide gums hydrogels with propolis extract as novel functional natural biomaterials. *International Journal of Biological Macromolecules,* **211**, 410–424.

42. Malini, M., Thirumavalavan, M., Yang, W. -Y., Jiunn-FwuLee & Annadurai, G. (2015) A versatile chitosan/ZnO nanocomposite with enhanced antimicrobial properties. *International Journal of Biological Macromolecules,* **80**, 121-129.

43. Dananjaya, S. H. S., Kumar, R. S., Yang, M., Nikapitiya, C., Lee, J. & Zoysa, M. D. (2018) Synthesis, characterisation of ZnO-chitosan nanocomposites and evaluation of its antifungal activity against pathogenic Candida albicans. *International Journal of Biological Macromolecules,* **108**, 1281–1288.

44. Mostafa, M. H., Elsawy, M. A., Darwish, M. S. A., Hussein, L. I. & Abdaleem, A. H. (2020) Microwave-Assisted preparation of Chitosan/ ZnO nanocomposite and its application in dye removal. *Materials Chemistry and Physics,* **248**, 122914.

45. Wan, J., Al-Baldawy, A. S., Qu, S., Lan, J., Ye, X., Fei, Y. & Kang, J. (2022) Band alignment of ZnO-based nanorod arrays for enhanced visible light photocatalytic performance. *RSC Advances,* **12(42)**, 27189–27198.

46. Ramachandran, S. & Sivasamy, A. (2018) Nanocrystalline ZnO as a Visible Active Photocatalyst for the Degradation of Benzene-1,4-diol. *International Journal of Nanoscience,* **17**, 1760008.

47. Gao, X., Li, L., An, M., Zheng, T. & Ma, F. (2022) ZnO QDs and three-dimensional ordered macroporous structure synergistically enhance the photocatalytic degradation and hydrogen evolution performance of WO_3/TiO_2 composites. *Journal of Physics and Chemistry of Solids,* **165**, 110655.

48. Chin, Y. -H., Sin, J. -C., Lam, S. -M., Zeng, H., Lin, H., Li, H. & Mohamed, A. R. (2022) 0-D/3-D heterojunction composite constructed by decorating transition metal oxide nanoparticle on peony-like ZnO hierarchical microstructure for improved photodegradation of palm oil mill effluent. *Optik,* **260**, 169098.

49. Shao, D., Yu, M., Sun, H., Hu, T., lian, J. & Sawyer, S. (2013) High responsivity, fast ultraviolet photodetector fabricated from ZnO nanoparticle–graphene core–shell structures. *Nanoscale,* **5(9)**, 3664–3667.

50. Asok, A., Kulkarni, A. R. & Gandhi, M. N. (2014) Defect rich seed mediated growth: a novel synthesis method to enhance defect emission in nanocrystals. *Journal of Materials Chemistry C,* **2(9)**, 1691–1697.

51. Krishnaveni, Rajendran, Thambidurai & Sivalingam (2013) Industrial method of cotton fabric finishing with chitosan–ZnO composite for anti-bacterial and thermal stability. *Industrial Crops and Products,* **47**, 160–167.

52. Nomaan, A. T., Ahmed, A. A., Ahmed, N. M., Idris, M. I., Hashim, M. R. & Rashid, M. (2021) ZnO quantum dot based thin films as promising electron transport layer: Influence of surface-to-volume ratio on the photoelectric properties. *Ceramics International,* **47(9)**, 12397–12409.

53. Wang, J., Yu, S. & Zhang, H. (2019) Effect of surfactants on photoluminescence properties of ZnO synthesised by hydrothermal method. *Optik,* **180**, 20–26.

54. Han, N., Wu, X., Chai, L., Liu, H. & Chen, Y. (2010) Counterintuitive sensing mechanism of ZnO nanoparticle based gas sensors. *Sensors and Actuators B: Chemical,* **150(1)**, 230–238.

55. Zhen, Q., Gao, L., Sun, C., Gong, H., Hu, P., Song, S. & Li, R. (2018) Honeycomb-like TiO_2@GO nanocomposites for the photo-degradation of oxytetracycline. *Materials Letters,* **228**, 318–321.

56. Li, B., Wang, R., Shao, X., Shao, L. & Zhang, B. (2017) Synergistically enhanced photocatalysis from plasmonics and a co-catalyst in Au@ZnO–Pd ternary core–shell nanostructures. *Inorganic Chemistry Frontiers,* **4(12)**, 2088–2096.

57. Chen, D., Huang, S., Huang, R., Zhang, Q., Le, T. -T., Cheng, E. & Chen, Z. (2019) Convenient fabrication of Ni-doped SnO_2 quantum dots with improved photodegradation performance for Rhodamine B. *Journal of Alloys and Compounds,* **788**, 929–935.

58. Hosseini, S. M., Sarsari, I. A., Kameli, P. & Salamati, H. (2015) Effect of Ag doping on structural, optical, and photocatalytic properties of ZnO nanoparticles. *Journal of Alloys and Compounds,* **640**, 408-415.

59. Zhang, H., Wang, Y. & Zhai, C. (2022) Construction of a novel p-n heterojunction CdS QDs/$LaMnO_3$ composite for photodegradation of oxytetracycline. *Materials Science in Semiconductor Processing,* **144**, 106568.

60. Nguyen, T. -B., Thi, T. H. D., Thi, K. H. D., Minh, H. B., Thi, N. Q. N., Ngoc, D. V. & Dinh, B. N. (2022) N-TiO_2-δ/g-C_3N_4 dual photocatalysts for efficient oxytetracycline hydrochloride photodegradation and CO_2 photoreduction. *Adsorption Science & Technology*.

61. Moghni, N., Boutoumi, H., Khalaf, H., Makaoui, N. & Colón, G. (2022) Enhanced photocatalytic activity of TiO_2/WO_3 nanocomposite from sonochemical-microwave assisted synthesis for the photodegradation of ciprofloxacin and oxytetracycline antibiotics under UV and sunlight. *Journal of Photochemistry and Photobiology A: Chemistry,* **428**, 113848.

62. Zhang, S., Zhao, S., Huang, S., Hu, B., Wang, M., Zhang, Z., & Du, M. (2021) Photocatalytic degradation of oxytetracycline under visible light by nanohybrids of CoFe alloy nanoparticles and nitrogen-/sulfur-codoped mesoporous carbon. *Chemical Engineering Journal,* **420**, 130516.

63. Wang, J., Zang, L., Wang, L., Tian, Y., Yang, Z., Yue, Y. & Sun, L. (2022) Magnetic cobalt ferrite/reduced graphene oxide (CF/rGO) porous balls for efficient photocatalytic degradation of oxytetracycline. *Journal of Environmental Chemical Engineering,* **10(5)**, 108259.

64. Guo, L., Xu, F., Liu, Z., Zhang, M., Ma, D., Lai, C. & Qin, L. (2020) Constructing benzene ring modified graphitic carbon nitride with narrowed bandgap and enhanced molecular oxygen activation for efficient photocatalytic degradation of oxytetracycline. *Separation and Purification Technology,* **294**, 121170.

65. Ouyang, K., Xu, B., Yang, C., Wang, H., Zhan, P. & Xie, S. (2022) Synthesis of a novel Z-scheme Ag/WO_3/g-C_3N_4 nanophotocatalyst for degradation of oxytetracycline hydrochloride under visible light. *Materials Science in Semiconductor Processing,* **137**, 106168.

66. Feng, C., Lu, Z., Zhang, Y., Liang, Q., Zhou, M., Li, X. & Xu, S. (2022) A magnetically recyclable dual Z-scheme GCNQDs-$CoTiO_3$/$CoFe_2O_4$ composite photocatalyst for efficient photocatalytic degradation of oxytetracycline. *Chemical Engineering Journal,* **435**, 134833.

67. Li, T., He, H., Zhang, P., Zhao, X., Yin, W. & Tu, X. (2022) The synergy of step-scheme heterojunction and sulfur vacancies in $AgInS_2$/$AgIn_5S_8$ for highly efficient photocatalytic degradation of oxytetracycline. *Colloids and Surfaces A: Physicochemical and Engineering Aspects,* **646**, 128946.

68. Xue, L., Liang, E. & Wang, J. (2022) Fabrication of magnetic ZnO/$ZnFe_2O_4$/diatomite composites: Improved photocatalytic efficiency under visible light irradiation. *Journal of Materials Science: Materials in Electronics,* **33**, 1405–1424.

69. Vaizoğullar, A. I. (2019) ZnO/ZrO_2 composites: Synthesis characterisation and photocatalytic performance in the degradation of oxy tetracycline antibiotic. *Advanced Performance Materials,* **34(8)**, 433–443.

70. Falamas, A., Marica, I., Popa, A., Toloman, D., Pruneanu, S., Pogacean, F. & Stefan, M. (2022) Size-dependent spectroscopic insight into the steady-state and time-resolved optical properties of ZnO photocatalysts. *Materials Science in Semiconductor Processing,* **145**, 106644.

71. Toloman, D., Popa, A., Stan, M., Stefan, M., Vlad, G., Ulinici, S. & Pana, O. (2021) Visible-light-driven photocatalytic degradation of different organic pollutants using Cu doped ZnO-MWCNT nanocomposites. *Journal of Alloys and Compounds*, **866**, 159010.